Supplementary Information (SI) for Dalton Transactions.

A Drive Towards Bi-Linker Strategy: Tailoring MOF Efficiency for Advanced Battery-Supercapacitor Hybrid Devices

Junaid Khan[a, b, d, *], Anique Ahmed[c], Abdullah A. Al-Kahtani[e]

[a]Department of Physics, Government Postgraduate Collage No.1, Abbottabad, Khyber Pakhtunkhwa, Pakistan

[b]Department Of Higher Education Achieves and Libraries, Government of Khyber Pakhtunkhwa, Pakistan

[c]Faculty of Engineering Sciences, GIK Institute of Engineering Sciences and Technology, Topi 23640, Khyber Pakhtunkhwa, Pakistan

[d]Department of Chemical and Bilogical Engineering, Gachon University, 1342 Seongnam-daero, Seongnam13120, Republic of Korea

[e]Chemistry Department, Collage of Science, King Saud University, P. O. Box 2455, Riyadh-22451, Saudi Arabia

*Email: junaidkhan.nanotech@gmail.com

Fig. S1: SEM images of X1-X5 at high resolution.

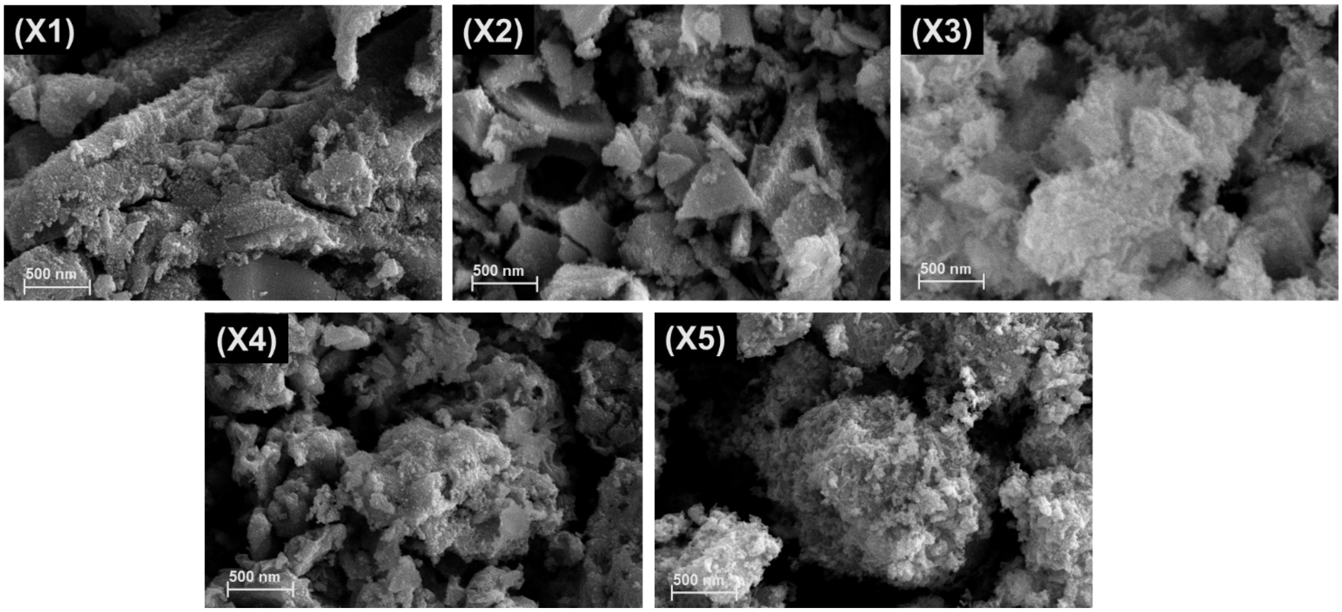

Fig. S2: Elemental mapping was performed using energy-dispersive X-ray spectroscopy (EDS) coupled with scanning electron microscopy (SEM) for the optimum sample X2. The elemental maps clearly demonstrate the homogeneous dispersion of key elements including nickel (Ni), carbon (C), oxygen (O), and nitrogen (N) throughout the MOF matrix. The presence of nitrogen, attributed solely to the pyridine functionality of the PDC linker, served as a qualitative marker to track its incorporation. Simultaneously, the enhanced carbon and oxygen signals correspond to the aromatic and carboxylic functionalities of both linkers. The consistent elemental distribution supports the successful formation of a uniform bimetallic organic framework and affirms the effectiveness of the bi-linker strategy in synthesizing a compositionally controlled MOF structure.

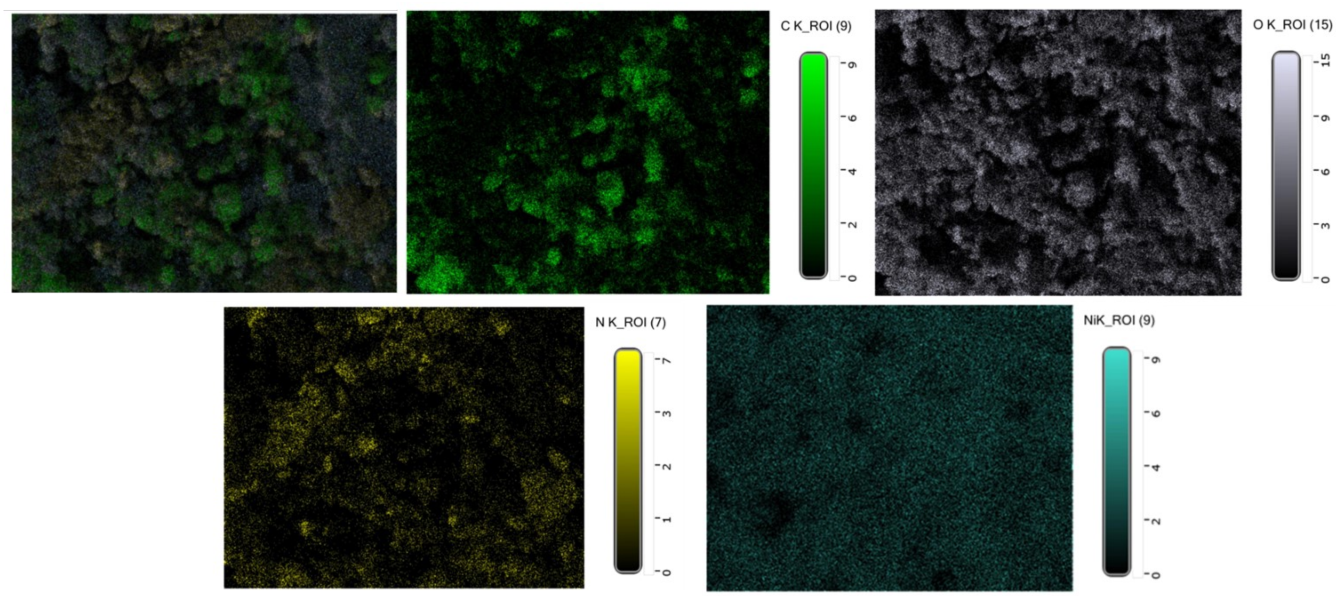

Fig. S3: The Brunauer-Emmett-Teller (BET) analysis of the synthesized samples (X1 to X5).

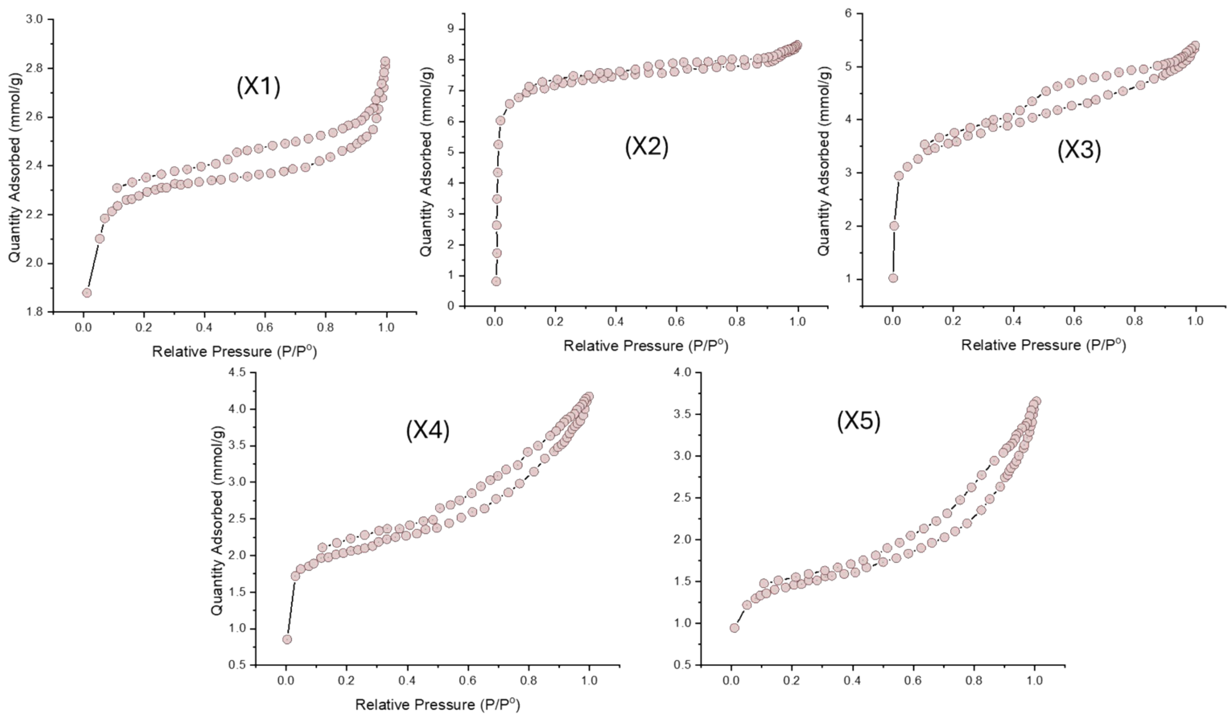

Fig. S4: CV profile of activate carbon and optimized Ni MOF X2 in three cell configurations.

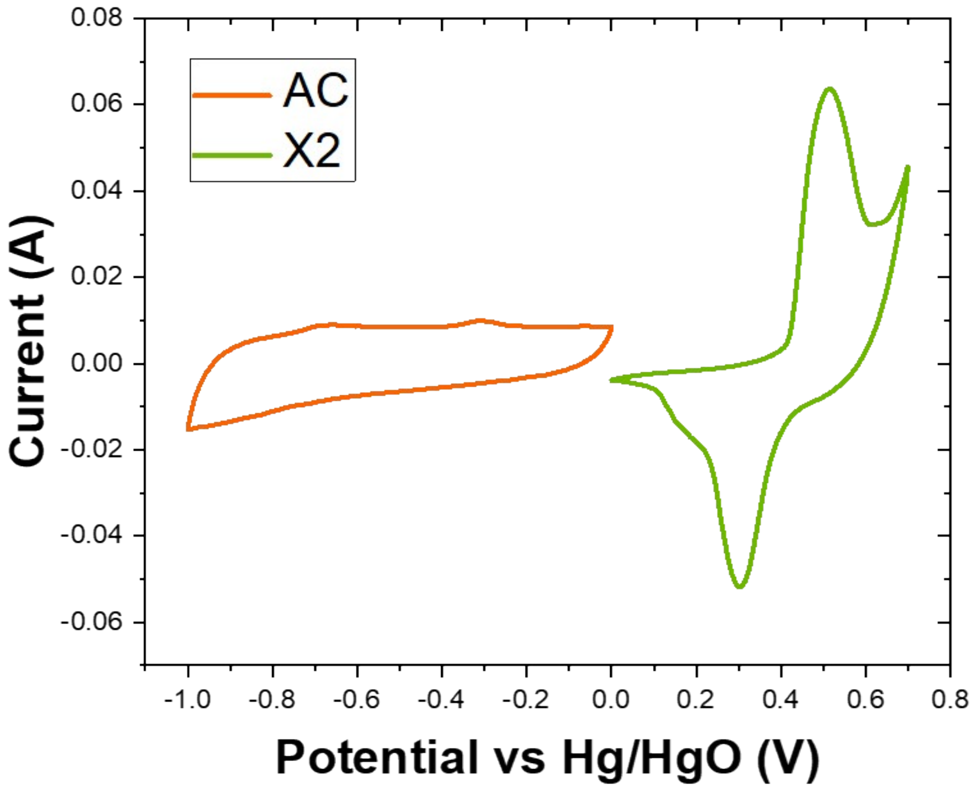

Fig. S5: CV profile of real device being reliably operated within multiple potential ranges.

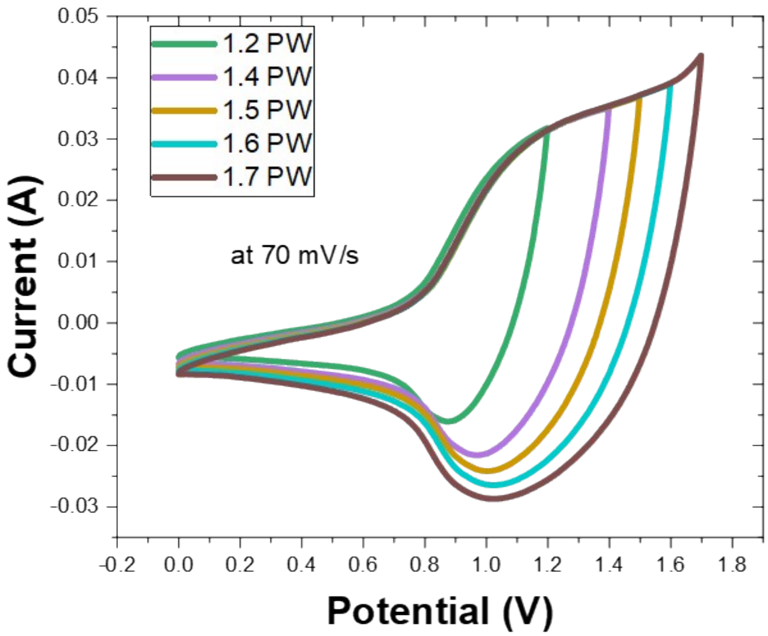

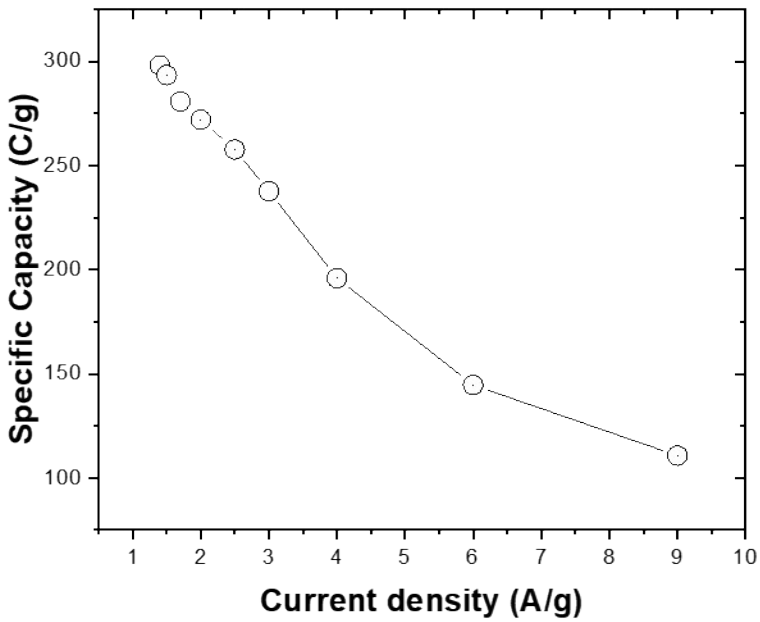

Fig. S6: Specific capacity of real device calculated from GCD curves.

Fig. S7: Capacitive and diffusive contribution was scrutinized using experimental CV data of real device, **(a)** capacitive and diffusive contribution is plotted against the experimental CV results at 10 mV/s, **(b)** percentage of both charge storage mechanisms at multiple scan rates.

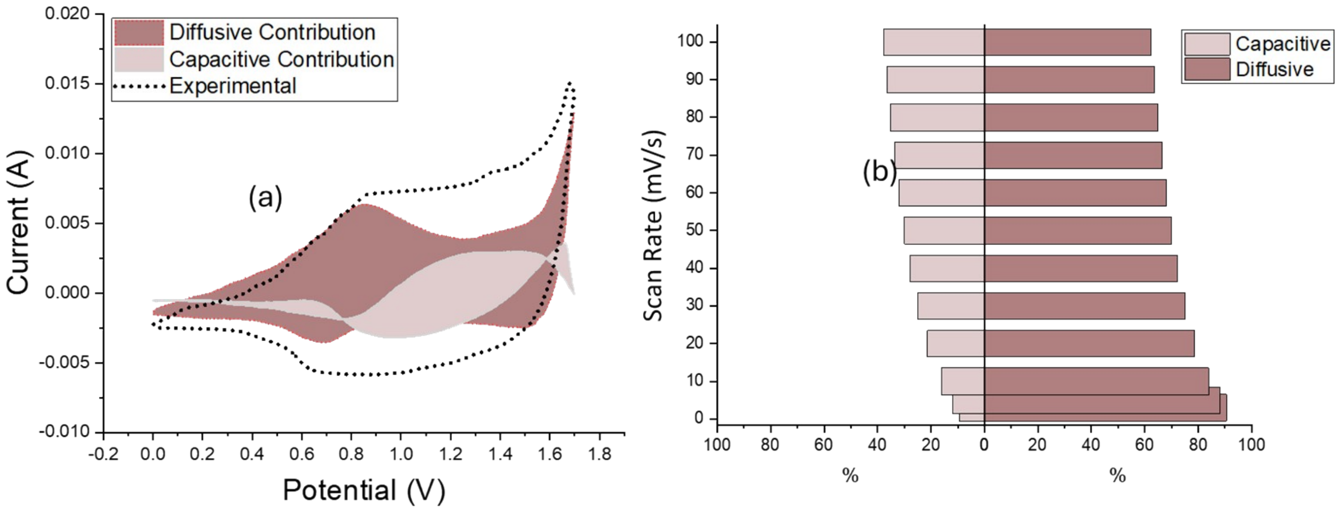

The charge storage capability in terms of specific capacity of the corresponding electrode was also depicted utilizing CV outcomes while employing the following relation:

$$Q_s = \frac{1}{m\mathrm{V}}\int_{Vi}^{Vf} I \times dV \qquad (1)$$

The Q_s signify the specific capacity (C/g). The active mass of electrode material (g), scan rate (V/s), and voltage (V) are represented by m, V, and V respectively.

The GCD results have further opted to scrutinize storage capability as:

$$Q_s = \frac{I \times \Delta t}{m} \qquad (2)$$

$$C_s = \frac{I \times \Delta t}{m \times \Delta V} \qquad (3)$$

Here 'C_s' and 'Δt' represent the specific capacitance (F/g) and discharge time (s) correspondingly.